AD-A106 106 WASHINGTON UNIV ST LOUIS MO SEMICONDUCTOR RESEARCH LAB F/G 20/2
IMPURITY AND DEFECT INTERACTIONS IN GAAS.(U)
SEP 81 C M WOLFE, P A FEDDERS, G E STILLMAN N00014-80-C-0762
UNCLASSIFIED 64422-1 NL

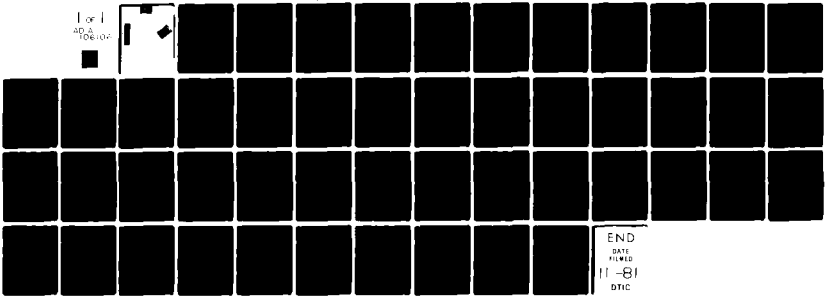

Unclassified

SECURITY CLASSIFICATION OF THIS PAGE (When Data Entered)

REPORT DOCUMENTATION PAGE	READ INSTRUCTIONS BEFORE COMPLETING FORM
1. REPORT NUMBER	2. GOVT ACCESSION NO. AD-A106196 / 3. RECIPIENT'S CATALOG NUMBER
4. TITLE (and Subtitle) Impurity and Defect Interactions in GaAs,	5. TYPE OF REPORT & PERIOD COVERED Annual Technical Report 1 Aug 80-31 Jul 81
	6. PERFORMING ORG. REPORT NUMBER 64422-1
7. AUTHOR(s) C.M. Wolfe, P.A. Fedders, G.E. Stillman, Camellia M.L. Yee, R.T. Green and T.S. Low	8. CONTRACT OR GRANT NUMBER(s) N00014-80C-0762
9. PERFORMING ORGANIZATION NAME AND ADDRESS Semiconductor Research Laboratory Box 1127 Washington University St. Louis, MO 63130	10. PROGRAM ELEMENT, PROJECT, TASK AREA & WORK UNIT NUMBERS PE 61153N RR 021-02-03 NR 243-034
11. CONTROLLING OFFICE NAME AND ADDRESS Office of Naval Research Code 414 Arlington, VA 22217	12. REPORT DATE 30 Sep 1981
	13. NUMBER OF PAGES 46
14. MONITORING AGENCY NAME & ADDRESS (if different from Controlling Office)	15. SECURITY CLASS. (of this report) Unclassified
	15a. DECLASSIFICATION/DOWNGRADING SCHEDULE

16. DISTRIBUTION STATEMENT (of this Report)

Approved for public release; distribution unlimited.

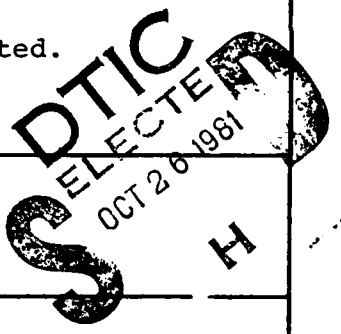

17. DISTRIBUTION STATEMENT (of the abstract entered in Block 20, if different from Report)

18. SUPPLEMENTARY NOTES

ONR Scientific Officer
Telephone: (202) 696-4218

19. KEY WORDS (Continue on reverse side if necessary and identify by block number)

GaAs, impurities, defects, complexes, epitaxy, ion implantation, Cr redistribution, impurity incorporation, complex formation, lineshape analysis.

20. ABSTRACT (Continue on reverse side if necessary and identify by block number)

The construction of an epitaxial reactor to examine the basic aspects of complex formation in GaAs has been completed. This reactor is designed to simultaneously dope the growing layer with a donor impurity and Cr and/or O so that impurity interaction regions are obtained in the same sample. We are currently calibrating this system for several dopants.

The redistribution of Cr during the annealing of uniform and

DD FORM 1 JAN 73 1473 EDITION OF 1 NOV 65 IS OBSOLETE

Unclassified

SECURITY CLASSIFICATION OF THIS PAGE (When Data Entered)

20. ABSTRACT (Continued)

ion-implanted bulk samples has been examined. Preliminary results indicate that the Cr build-up at the surface can be modified by applying an electric field to the surface during the annealing process.

For ion-implanted samples the pile-up of Cr in the implanted region appears to be strongly dependent on the annealing temperature for a given ion dose. The results suggest that this pile-up is due to an electrostatic interaction between the Cr and the implanted ions.

With the availability of high-purity GaAs from a variety of epitaxial growth techniques, improved donor identifications have been made by far infrared photoconductivity measurements. Samples grown by $AsCl_3$-H_2 VPE, $AsCl_3$-N_2 VPE, AsH_3 VPE, LPE, MBE, and MOCVD have been examined and the common residual donors have been identified.

A study of these far infrared photoconductivity donor spectra in a magnetic field indicates several features which are inconsistent with a second order Stark-shifted lineshape. It appears that many of the shallow donors have lower symmetry than the atoms they replace. This could be due to donor atoms displaced from simple substitutional sites or hydrogenic donor complexes. An analysis of these effects is expected to provide a powerful tool for determining the structure and electrical environment of the donors.

TABLE OF CONTENTS

1. RESEARCH OBJECTIVES

The purpose of this work is to investigate the interactions among impurities, defects, and complexes in GaAs which adversely affect the yield and performance of high-speed GaAs integrated circuits. To achieve this objective the following experimental approach is being employed: Impurities are introduced into GaAs by gas-phase doping during epitaxial growth and by ion-implantation into bulk samples. Annealing is performed under controlled atmospheres with applied electric, magnetic, or stress fields. The resulting samples are characterized by a combination of low and high temperature resistivity and Hall measurements, differential capacitance measurements, far and near infrared photoconductivity measurements, photoluminescence, electron spin resonance, and secondary ion mass spectroscopy. These data are then analyzed with impurity incorporation, redistribution, complex formation, and other models.

2. EPITAXIAL GROWTH WITH MULTIPLE DOPANTS

To examine the basic interactions and complex formation in GaAs, two types of epitaxial samples are being employed.

The first are thick epitaxial layers with low residual impurity concentrations. These are doped with known donors and Cr and/or O at levels up to about $1 \times 10^{16} cm^{-3}$. The substrates are removed from these thick layers to obtain samples suitable for high-temperature resistivity and Hall, far-infrared photoconductivity, and electron spin resonance measurements. Since all the other experimental methods can be applied to these samples as well, they provide the basic calibration for impurity and defect interactions.

The second type of epitaxial samples are thinner layers grown on heavily-doped substrates. These are doped non-uniformly with known donors and Cr and/or O in the following manner; (1) First, one impurity is introduced into the gaseous phase during growth to obtain a uniform doping level. (2) Then, a second impurity is introduced at a uniform level. (3) Finally, the first impurity source is turned off. These samples are designed for differential capacitance (C-V) measurements and secondary ion mass spectroscopy (SIMS) which provide depth information. The uniformly-doped regions for each impurity provide a calibration for the SIMS data in the overlapping double-doped region,

while the C-V data monitor the electrical activity in all three regions. The advantage of this approach is that each impurity interaction experiment is self-calibrated. Also, the effects of coulombic forces between impurities can be separated from other interaction forces by using doping levels both below and above the intrinsic carrier concentration.

2.1 UNIFORM DOPING

The reactor to prepare uniformly-doped samples is a standard $AsCl_3$-H_2 vapor phase system with one doping input line. Multiple doping is achieved by adding one or more impurities to the Ga melt while simultaneously introducing an additional impurity into the gaseous phase through the doping input line. The doping line is configured with a bubbler so that CrO_2Cl_2 (chromyl chloride) or H_2O can be used. Also, the bubbler can be bypassed to introduce gaseous dopants such as H_2S. Other donor impurities or Cr can be added to the Ga melt.

At the present time, a number of samples with a single dopant have been grown in this reactor to calibrate the far infrared photoconductivity and the electron spin resonance measurements.

2.2 OVERLAPPING PROFILE DOPING

The reactor used for the growth of self-calibrating epitaxial layers is shown in Figure 1. The system consists of a quartz reaction tube situated in a three-zone clamshell

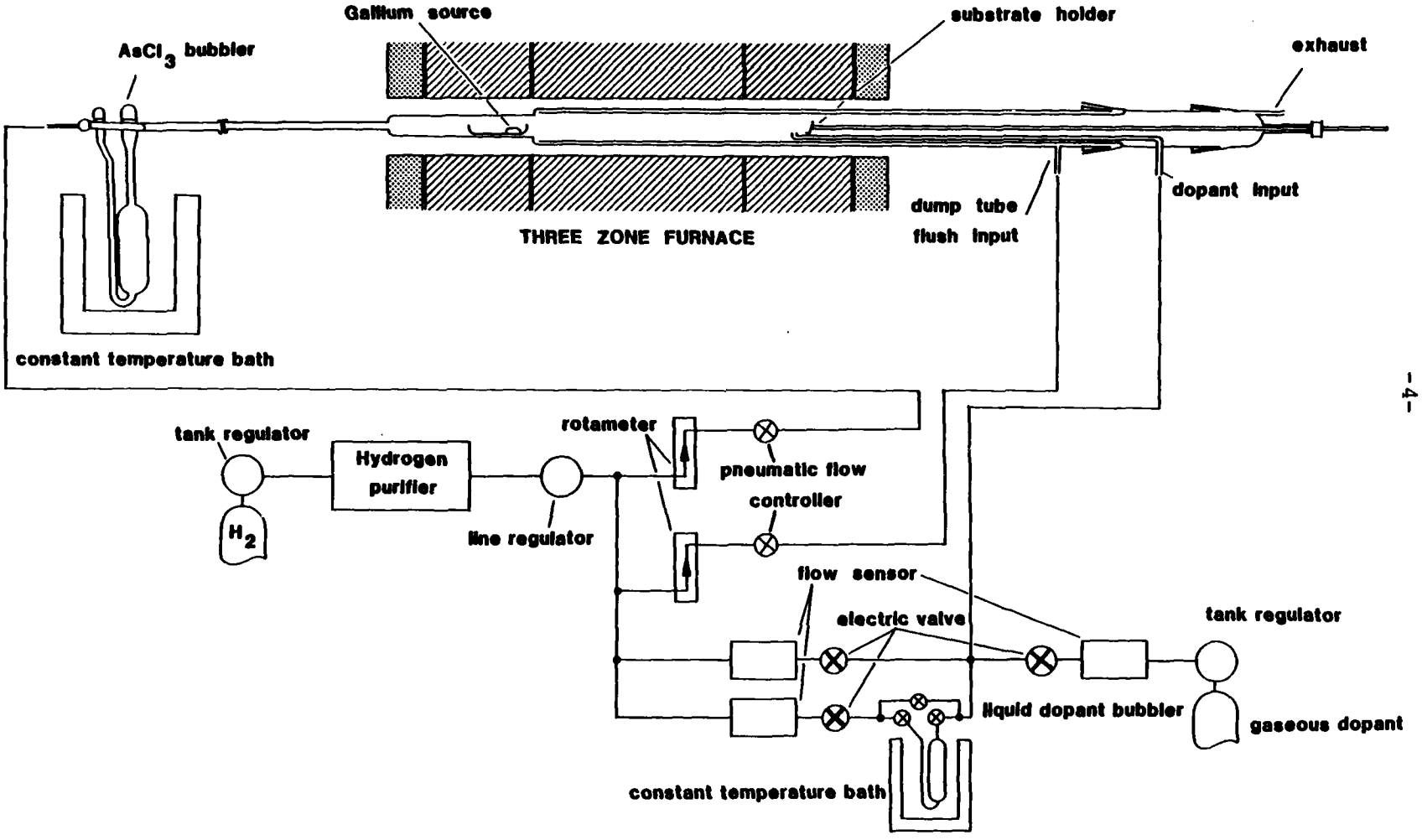

Figure 1. Epitaxial reactor to obtain overlapping doping profiles for self-calibrating samples.

furnace. The end zones of the furnace are equipped with variable length control thermocouples adjusted to give a four inch constant temperature zone along the axis of the reaction tube in which the Ga source is placed. The temperature gradient at the substrate holder is adjusted to be $20^{o}C$/inch.

The reaction tube is fabricated entirely from fused quartz tubing. Input to the reaction tube is achieved using a 10mm OD tube joined to a 33mm OD tube at the point where the reaction tube enters the furnace. Downstream of the Ga source, the reaction tube diameter again increases to accomodate a 40mm ID dump tube with a 1mm separation between dump tube and the 50mm OD outer wall of the reaction tube. The volume between the dump tube and the outer wall of the reactor is constantly flushed with high-purity H_2 introduced through a 6mm quartz tube in the outer wall of the reaction tube. The reaction tube is terminated with a 55/50 male taper joint and the dump tube is held in position by means of a ring seal to a 55/50 female taper joint. The 55/50 female taper joint is then connected to a 50/50 male taper joint through which the substrate may be inserted. The reaction tube is capped with a pyrex 50/50 female taper joint fitted so the substrate holder may be sealed in the proper position using an Ultra Torr, O-ring fitting. The endcap is also equipped with a 6mm exhaust line.

The $AsCl_3$ used in the system is held in a pyrex bubbler in the form of a U-tube valved at both ends so the $AsCl_3$ may be isolated completely from the gas flow. A bypass line also provides a continuous H_2 flow through the reaction tube. The $AsCl_3$ bubbler is connected to the reaction tube by means of a teflon-O ring fitting (solv-seal joint). The input to the bubbler is a controlled amount of high-purity H_2 through a 6mm pyrex tube. The partial pressure of $AsCl_3$ introduced into the reaction tube is controlled by varying the temperature of the ethanol-water bath surrounding the bubbler.

The dopants for the system are introduced near the substrate using a 6mm quartz tube attached to the inside of the dump tube. The system is currently set up to use both a gaseous and a liquid dopant. The liquid dopant is contained in an identical bubbler as that used for the $AsCl_3$. In addition to the two dopant lines going to the dopant input, there is also a H_2 line to dilute the dopants. Control for the impurity gas flows and the H_2 dilution line is obtained using a gas ratio mass flow controller system.

In fabricating this reactor, special consideration was given to the effect of potential dopants on the system. The dump tube was made necessary by the decision to use CrO_2Cl_2 as a source of Cr in the system. The Cr degrades the quartz at high temperatures making it extremely fragile. Thus a replaceable inner sleeve is required to prevent damage to the reactor. The choice of H_2S as a dopant

dictates the use of the Al tubing in the dopant input line to assure that consistent S doping can be achieved. Also, the lengths of tubing and dead spaces in the doping input lines are minimized to reduce the turn off and turn on times for the dopants.

The system is currently committed to O and S doping using H_2O and H_2S as the respective sources for the dopants.

3. CHROMIUM REDISTRIBUTION DURING ANNEALING

One of the main problems encountered in the fabrication of GaAs integrated circuits by ion implantation into Cr-doped substrates is the redistribution of the Cr during subsequent annealing. During the annealing process the Cr tends to move to the outer surface and also to build-up in the vicinity of the implanted ions. In an attempt to understand and, hopefully, eliminate these effects, annealing experiments with applied electric, magnetic, and stress fields are being performed.

3.1 ACCUMULATION AT SURFACES

It is known that surface states give rise to an electric field at the surface that can cause impurity redistribution at elevated temperatures [1]. In particular, it has been found that Cr tends to build up at the surface of epitaxial layers grown on Cr doped substrates. We are currently performing experiments to see if the electric field at the surface is a major factor in the build-up of Cr at the outer surface during annealing.

Briefly, these experiments utilize the MOS structure shown in Figure 2. The GaAs serves as ground. Three Al pads were evaporated onto the SiO_2 to serve as contacts for the applied voltage. Voltages of +V, 0, and -V are applied to the three pads during annealing. After the annealing period, the SiO_2 and Al are removed. SIMS measurements are then used to determine the Cr distribution in each area.

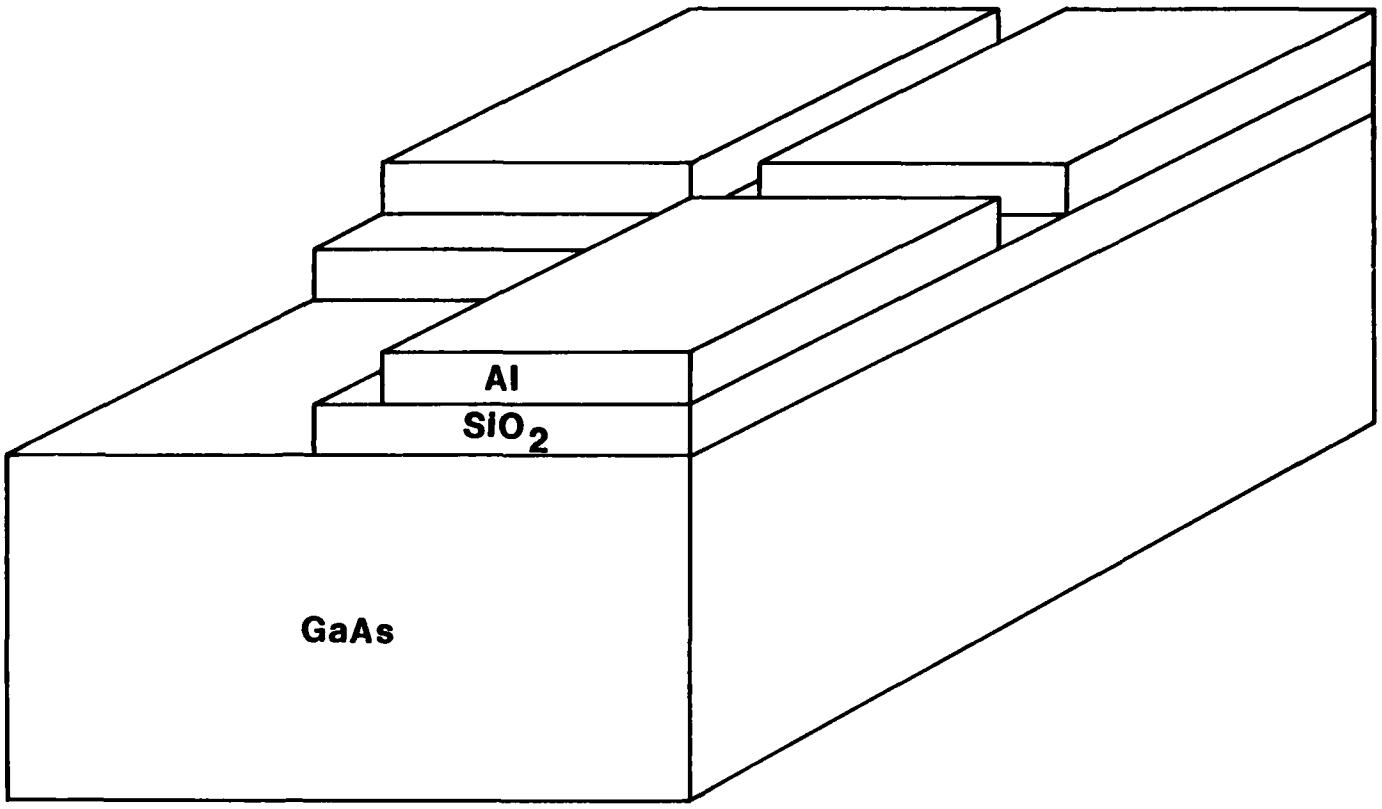

Figure 2. MOS structure used to examine the effects of an applied electric field on the accumulation of Cr near the surface of a Cr-doped substrate.

The samples consisted of both Cr-doped substrates and thin high mobility epitaxial layers grown on Cr doped substrates. A layer of SiO_2 was pyrolytically deposited on the back and front of each sample. The sample was then mounted face up on a glass slide with blackwax. The front-side was masked with blackwax except for the corner to be used as a ground contact to the GaAs substrate. A buffered HF etch was applied to remove the SiO_2 from the exposed window and the sample was rinsed in deionized water. The front surface was then flushed with trichloroethylene to remove the blackwax mask. The exposed window was masked off with blackwax and three additional areas were delineated with blackwax strips. Approximately 500 Å of Al was evaporated onto the sample. The sample was then allowed to soak in trichloroethylene to remove all traces of blackwax and to lift off the Al deposited on the masked off areas. Finally, the sample was cleaned with trichloroethylene, acetone, and methanol to give the structure in Figure 2.

The apparatus used to anneal the samples is shown in Figure 3. The molybdenum wires and carbon probes provided ohmic contacts to the exposed GaAs and the Al pads at 600°C. After each sample was mounted in the furnace tube, the tube was flushed with H_2 for 15 minutes. During this time, the molybdenum wires were connected to two power sources to provide the proper biases of +V, O, and -V with the contact to the exposed GaAs window grounded.

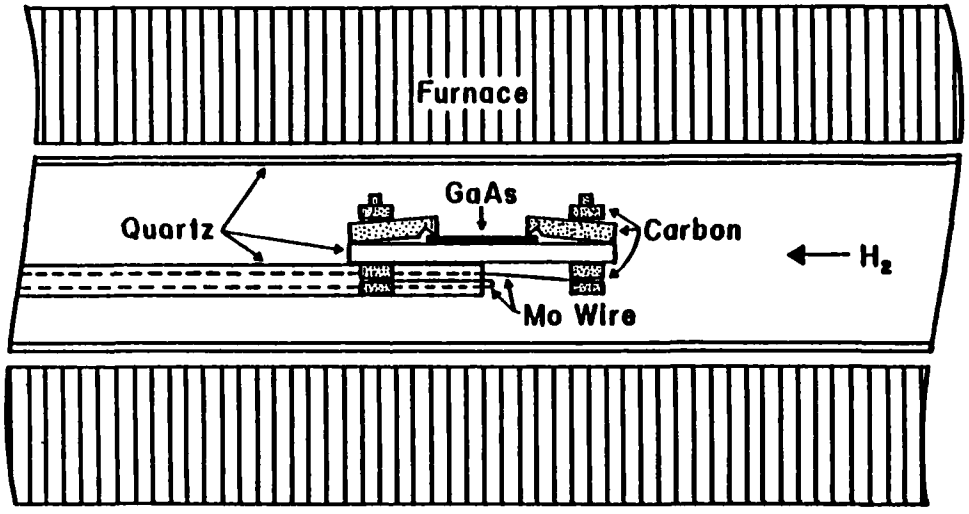

Figure 3. High-temperature annealing furnace with provision for electrical contacts.

The samples were situated in a flat temperature zone at 600°C. A half hour warmup was sufficient to establish a stable furnace profile. The samples were then annealed for eight hours. After an appropriate cooling period, the samples were removed from the furnace. They were then flushed with HF etch to remove the Al and SiO_2 from all surfaces. A final deionized water rinse was used to quench the HF etch.

An attempt was made to do a zero-bias capacitance measurement on each sample. However, the resistivities of the samples were too high for any measurements to be made. SIMS measurements were done at C.A. Evans & Associates. Preliminary results indicate that the amount of Cr buildup at the surface is dependent on the applied voltage. In one case, there was a depletion of Cr at the surface. At the present time we have not looked at sufficient samples to draw any quantitative conclusions.

3.2 ACCUMULATION IN ION IMPLANTED REGIONS

In addition to the Cr build-up at the outer surface during annealing, there are also problems associated with Cr accumulation in the vicinity of the implanted ions. Recently, a number of workers [2-13] have examined this problem and we have summarized most of these data in Figure 4.

This figure is a plot of the peak concentration of the implanted ion profile as determined by SIMS measurements versus the temperature at which the Cr-doped substrates

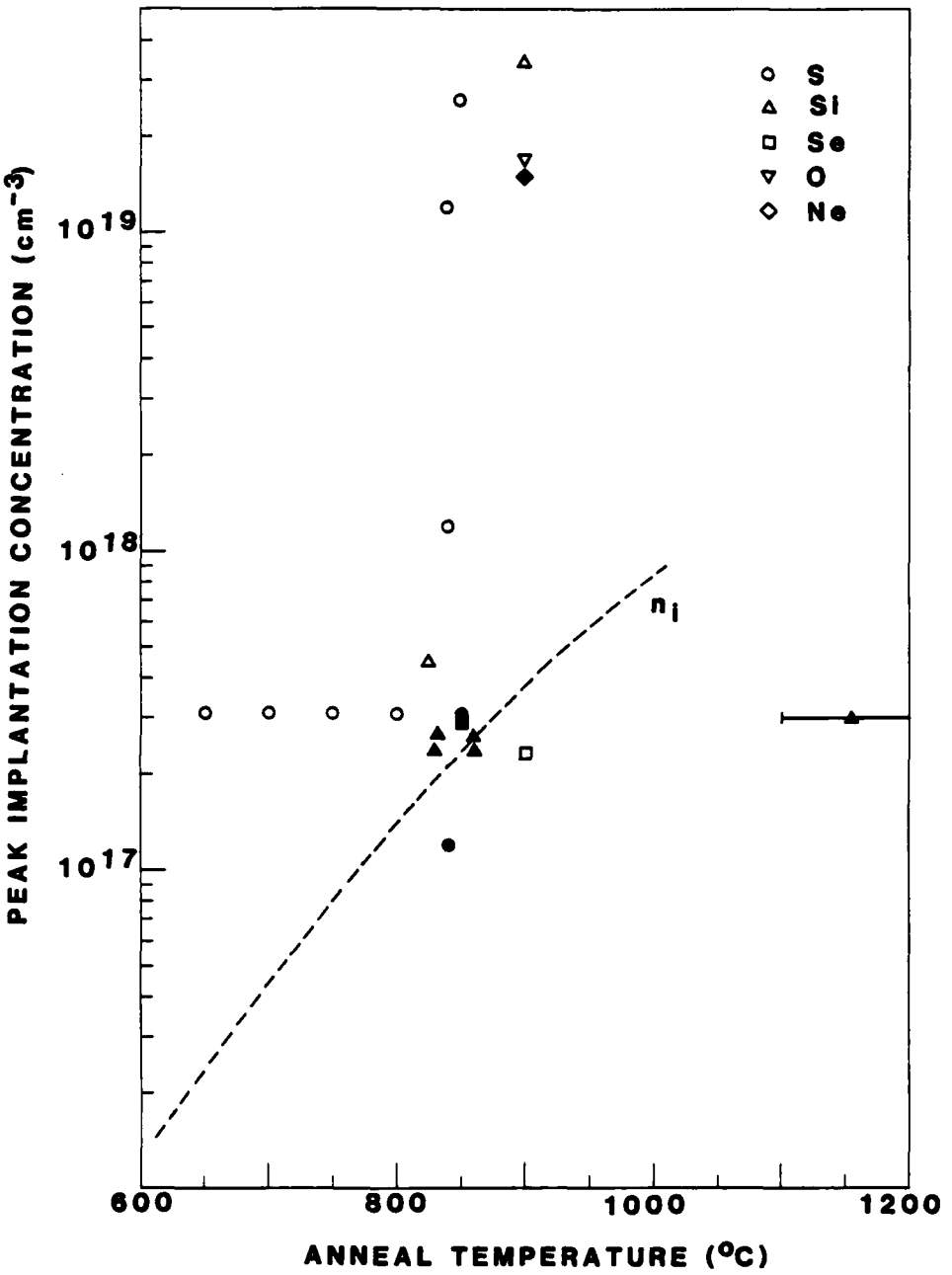

Figure 4. Peak ion implantation concentration vs. annealing temperature for Cr-doped substrates. The open symbols indicate Cr build-up in the implanted regions, while the solid symbols indicate no Cr build-up.

were annealed to activate the ions. The open symbols in the figure indicate samples in which the Cr accumulated in the vicinity of the ions, while the solid symbols indicate samples in which the Cr did not. (In many of the latter samples, in fact, the Cr depleted from this region and accumulated at the surface). The solid symbol with a temperature error bar was a laser-annealed sample [13] for which we estimated the temperature. The dashed line in Figure 4 is the measured [14] intrinsic carrier concentration of GaAs as a function of temperature.

Notice that, with the exception of a Ne implanted sample [10], all of the samples in which Cr build-up was not observed are near or below the intrinsic concentration line. This suggests the following explanation for the accumulation of Cr in implanted regions: (1) With the exception of Ne, the implanted ions are electrically activated during the annealing process. (2) The electrons associated with these ions diffuse in their concentration gradients producing space-charge regions and electric fields. (3) The mobile Cr ions in the substrate then accumulate in these field regions. (4) If, however, annealing is performed at temperatures where the intrinsic carrier concentration is greater than the carrier concentration associated with the implanted ions; no space-charge regions, no electric fields, and no Cr accumulation is observed.

The peak concentration data in Figure 4 was obtained by SIMS measurements which measure the total number of impurity atoms. Thus, if only the concentration of activated impurities is taken into account, it is possible that all of the solid symbols in Figure 4 would fall below the intrinsic line. It should also be pointed out that we have not included B implantation data [6,7,11] or very high dose implants [15] in Figure 4. For these samples several interesting effects are observed, which are related to the damage induced by the heavy ion doses. At lower doses, however, the data suggest that the Cr pile up is due to an electrostatic interaction between the Cr and the implanted ions.

4. FAR INFRARED PHOTOCONDUCTIVITY EXPERIMENTS

4.1 PHOTOTHERMAL IONIZATION OF DONORS

The nearly hydrogenic energy level spectra of residual donors in high purity GaAs have been studied by several groups using photothermal ionization spectroscopy. Since the donor ground state energy differs slightly from the value predicted from hydrogenic theory, and since this difference is donor species dependent, each hydrogenic transition in a photothermal ionization spectrum contains several closely spaced peaks. Each peak corresponds to a particular donor species present, and has an amplitude which is a measure of the relative concentration of that donor species. This multiplet structure is most easily resolved at high magnetic fields (about 5 T) in the hydrogenic 1s-2p(m=-1) transition. For this reason, all the spectra which appear in this report show only this transition. The successful application of photothermal ionization spectroscopy requires that $N_D \lesssim 10^{15} cm^{-3}$ to avoid donor interaction. Photothermal ionization spectra have been recorded for high purity GaAs produced by $AsCl_3$-VPE, AsH_3-VPE, LPE, MBE, and MO-CVD growth techniques. The residual donors observed in such unintentionally doped GaAs are for the most part characteristic of the growth technique employed, and independent of the laboratory in which the samples were prepared. Electrical properties of the samples whose spectra are shown in the figures are given in Table 1.

Table 1. Electrical Properties

Figure	Sample	μ_{77} (cm^2/Vs)	n_{77} (cm^{-3})	t(μm)
2 (a)	$AsCl_3$-H_2 VPE (Wolfe)	201,000	4.5×10^{13}	56
2 (b)	$AsCl_3$-H_2 VPE (Ozeki *et al*)	95,000	3.0×10^{13}	20
2 (c)	$AsCl_3$-N_2 VPE (Ozeki *et al*)	132,000	2.0×10^{13}	20
3	AsH_3 VPE (Kennedy)	137,000	7.0×10^{13}	26
4	LPE (Tiwari *et al*)	129,000	1.2×10^{14}	14
5	MBE (Calawa)	108,000	6.3×10^{13}	5
6	MO-CVD (Dapkus *et al*)	106,000	2.1×10^{14}	30
7	$AsCl_3$-H_2-S VPE (Wolfe)	74,000	9.3×10^{14}	83

Results on high purity VPE growth of GaAs prior to 1970 have been reviewed previously [16]. At that time the only VPE technique that had produced high purity GaAs was the $AsCl_3$-Ga-H_2 vapor phase system. Epitaxial material with carrier concentrations of $n_{77} \approx 5 \times 10^{13} cm^{-3}$ and liquid nitrogen mobilities of $\mu_{77} \approx 200{,}000$ cm^2/Vs could be routinely produced. Because of the successful growth of extremely high purity GaAs by the $AsCl_3$-Ga-H_2 VPE system, much of the early donor identification work was done with material prepared by this technique. Wolfe *et al* [17] doped with Si, Ge, Sn, Pb, S, Se, and Te by adding a small amount of the dopant in elemental form to the Ga melt. They also attempted to dope with O by adding Ga_2O_3 to the melt, and with C by placing a high purity graphite source near the growing layer. By comparing the spectra of the lightly doped samples with those of unintentionally doped samples grown in the same reactor, identifications of spectral peaks in the 1s-2p (m=-1) transition with their chemical donor species could be made with reasonable certainty for Si, Ge, Sn, Pb, S, and Se. The identifications of C and Te were considered tentative, while O was apparently not incorporated as a donor. These identifications and the well established photothermal ionization peak positions are shown in Figure 5.

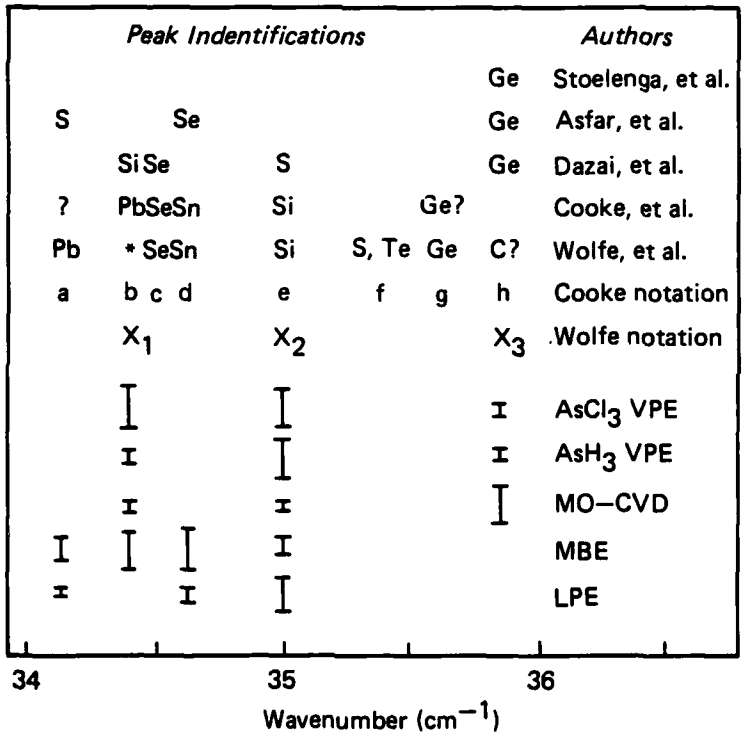

Figure 5. Characteristic donor peaks for GaAs grown by various techniques and several author's identifications. Vertical line heights indicate typical relative concentrations. (B=5.25 T).

A spectrum for an undoped $AsCl_3$-Ga-H_2 sample is shown in Figure 6 (a). The peaks X_1, X_2, and X_3 are the residual donors characteristic of this growth technique and the relative concentrations of these donors, indicated by the peak heights, are also typical.

A variation of the $AsCl_3$-Ga-H_2 technique, in which N_2 is used as the carrier gas instead of H_2, has been explored by Dazai *et al* [18]. Ozeki *et al* [19] grew samples using both techniques and found that, while samples grown with the H_2 carrier gas showed the usual three residual donors, X_1, X_2, and X_3, samples grown with N_2 as the carrier gas showed no evidence of X_1. These workers kindly loaned us samples, one grown with H_2, and one grown with N_2 carrier gas. Spectra for these samples appear in Figure 6 (b) and 6 (c), respectively. Since the position of the 1s-2p(m=-1) transition changes with magnetic field, all three of the spectra in Figure 6 were taken leaving the superconducting magnet in persistent mode, to facilitate comparison of peak positions between our standard sample in Figure 6 (a) and the other two samples. These measurements confirm the results of Ozeki *et al* [19] that X_1 is suppressed in the $AsCl_3$-Ga-N_2 VPE growth system.

While the chloride vapor phase growth technique has produced the highest purity GaAs, the hydride (AsH_3-Ga-HCl-H_2) growth technique is advantageous for the growth of GaInAsP alloys. Kennedy [20] has produced

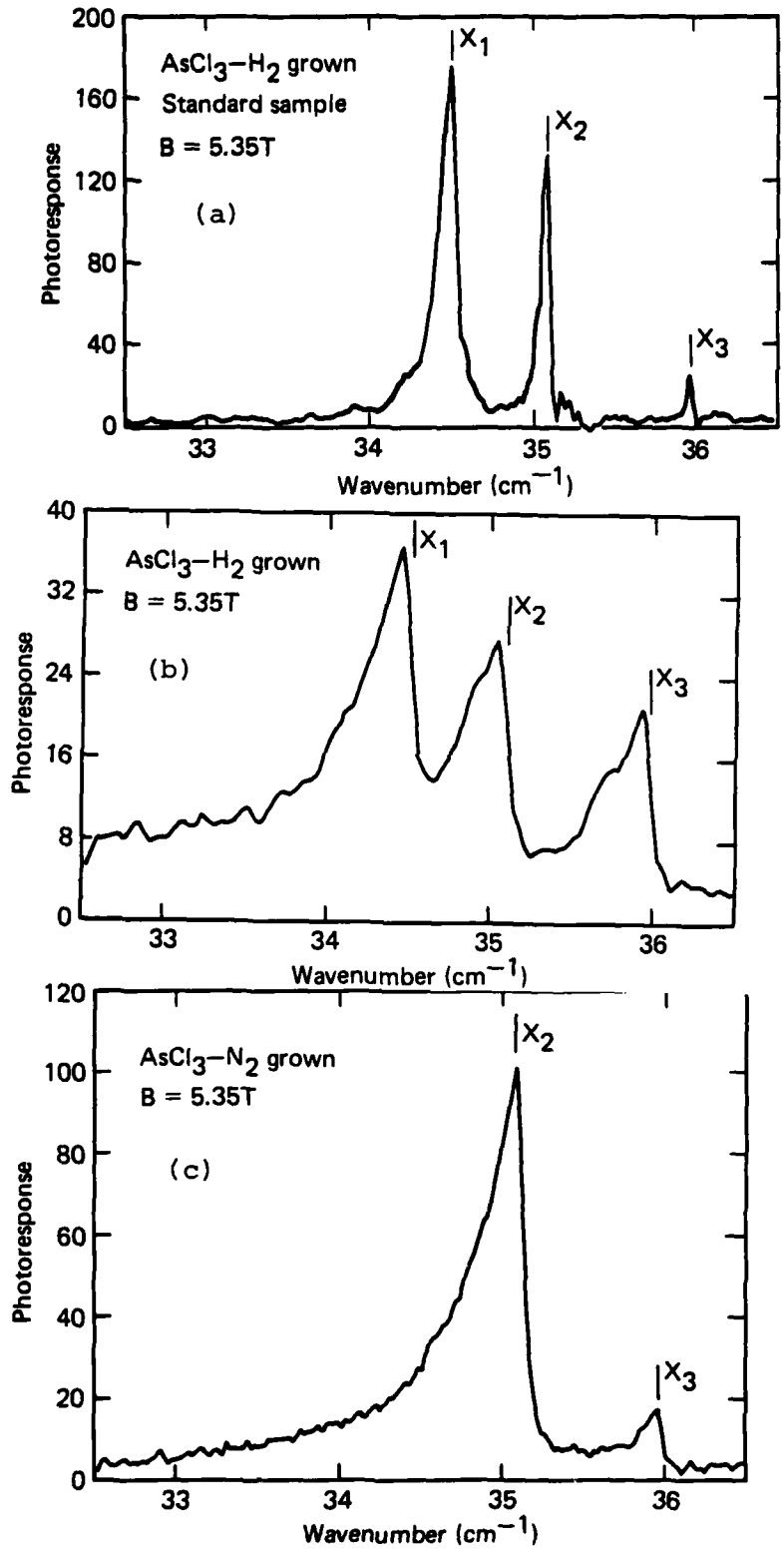

Figure 6. Spectra of $AsCl_3$ grown samples.

high purity GaAs epitaxial layers with $\mu_{77} \approx 167{,}000$ cm^2/Vs and more recently samples with $\mu_{77} \approx 200{,}000$ cm^2/Vs have been grown by Abrokwah [21]. Photothermal ionization spectra for several samples provided by both have shown the residual donors to be X_1, X_2, and X_3, with X_2 being dominant while the concentrations of X_1 and X_3 are sometimes quite small. A spectrum for a typical hydride VPE sample, grown by Kennedy is shown in Figure 7. The positions of the markers for X_1, X_2, and X_3, which appear in this and all the other figures were determined by comparison with a spectrum taken for our standard sample at precisely the same magnetic field.

There has been considerable effort in the LPE growth of high purity GaAs. Cooke *et al* [22] and Stradling [23] examined both undoped samples and samples doped with Sn, Pb, and Se, and confirmed the identifications for these dopants made by Wolfe *et al* [17]. The residual donors they observed in undoped LPE material from three different laboratories corresponded to Pb, Sn, and X_2 in roughly the ratios of 1:2:3. An example of spectra for high purity LPE GaAs samples grown by Tiwari and Eastman [24] is shown in Figure 8. As reported by Cooke *et al* [22] and also Morkoç *et al* [25] the dominant residual donors in these samples are Sn and X_2 with a smaller concentration of Pb. In addition, a peak due to X_2 is resolved in this spectrum, and while this is the first observation of X_1 in LPE GaAs,

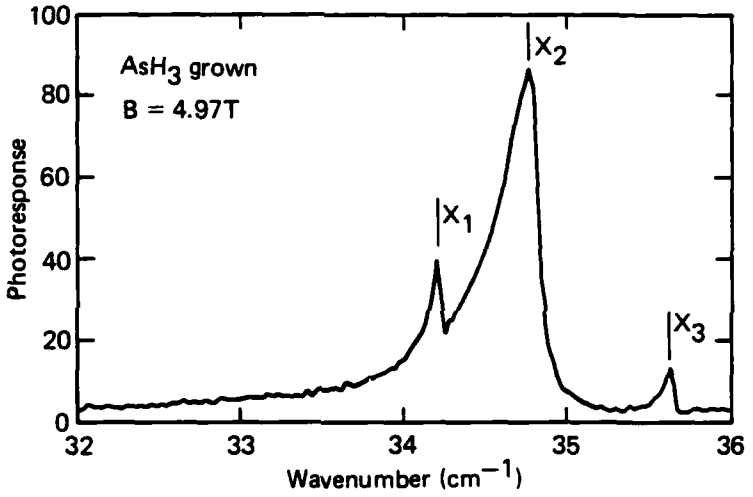

Figure 7. Photothermal ionization spectrum for Kennedy's AsH_3-VPE sample.

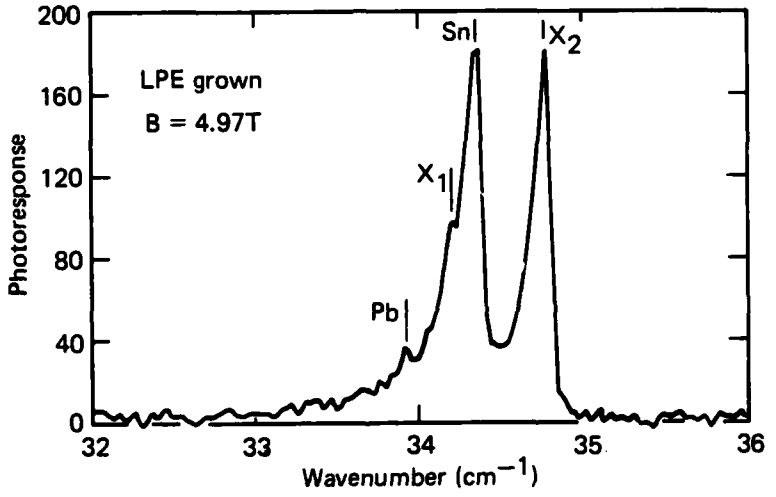

Figure 8. Photothermal ionization spectrum for Tiwari's *et al* LPE sample.

the proximity of the X_1 and the Sn peaks and the typically large residual Sn concentrations in LPE material may have prevented its observation in earlier work. In the spectrum of another undoped LPE GaAs sample grown by Abrokwah [21] Pb was absent and only traces of X_1 and Sn were detected leaving X_2 as the single dominant residual donor.

High purity unintentionally doped GaAs grown by MBE using a metallic As source is p-type. Using Sn doping Morkoç and Cho [26] produced a 27 μm thick n-type sample with a carrier concentration of $4 \times 10^{14} cm^{-3}$ and $\mu_{77} \approx 105{,}000\ cm^2/Vs$. The spectrum of this sample showed Pb, possibly X_1, and X_2, in addition to the intentionally added Sn. MBE samples grown by Collins [27] using a metallic As source but Si instead of Sn doping showed pronounced X_1 and smaller X_2 peaks in their photothermal ionization spectra. Unintentionally doped MBE samples grown by Calawa [28] using As provided by cracking AsH_3 as it entered the growth chamber were also measured. The layers grown in this way were n-type. Photothermal ionization spectra for these samples (Figure 9) showed the presence of Pb, Sn, and X_2, while X_1 was observed clearly in only one of the samples. The presence of Sn in these spectra is probably a result of previous use of Sn as a dopant in the same growth chamber.

The first report of high purity GaAs growth by MO-CVD was by Seki *et al* [29] who used triethylgallium as the

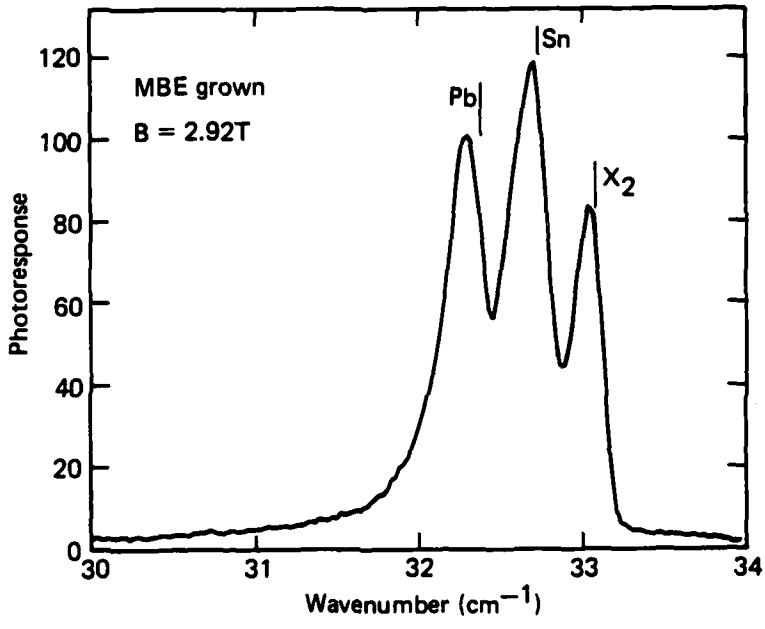

Figure 9. Photothermal ionization spectrum for Calawa's MBE sample.

metalorganic source to grow samples with $\mu_{77} \approx 125{,}000$ cm^2/Vs. Dapkus *et al* [30] subsequently prepared MO-CVD samples with μ_{77} as high as 125,000 cm^2/Vs using a trimethylgallium source. Spectra recorded for ten such unintentionally doped samples showed the dominant donor to be X_3. Only a trace of Pb was observed in one sample, while X_1, Sn, and X_2 were seen in concentrations which varied and occasionally became comparable to that of X_3, depending on growth parameters and source material. An example spectrum for this high purity MO-CVD material is shown in Figure 10. These results are to be compared with the earlier measurement of an alkyl grown sample by Cooke *et al* [22] who observed only Pb and X_3 in the ratio of 7 to 10.

4.2 IDENTIFICATION OF DONORS

There is general agreement in the literature on the energy at which photothermal ionization peaks occur, and for Pb, Sn, and Se the association of peaks with their chemical donor species is fairly well established. There is controversy, however, over the identification of some of the other peaks observed in GaAs.

In the work of Wolfe *et al* [17] the peak X_1 could not be correlated with a chemical donor species and, because this peak had not been observed in high purity LPE material, it was suggested that it might involve a stoichiometric defect (i.e a Ga vacancy (Stillman *et al* [31])). Recent annealing experiments on high purity GaAs have tended to

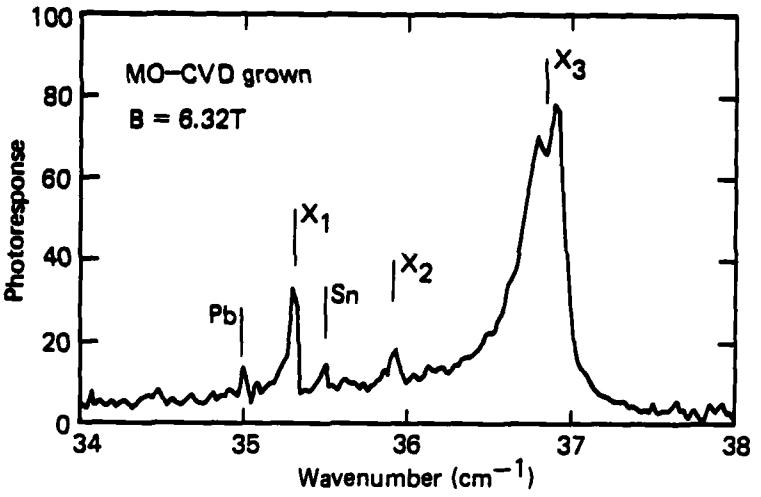

Figure 10. Photothermal ionization spectrum for Dapkus' *et al* MO-CVD sample.

support this identification (Stradling [23]). However, the presence of X_1 in undoped material grown in the $AsCl_3$-H_2 system, and its absence in that grown by the $AsCl_3$-N_2 system of Ozeki *et al* [19] suggest that X_1 might be associated with Si, in view of the expected role of H_2 in Si incorporation reactions. These authors observed the peak X_1 in a Si doped $AsCl_3$-N_2 grown sample and also observed a correlation between the appearance of X_1 and the presence of a Si peak in photoluminescence. Also, the MBE samples grown by Collins [27] in which Si doping was used to render the samples n-type, showed a dominant X_1 peak and a small X_2 peak in their spectra, and larger carrier concentration (indicating heavier Si doping) correlated with a larger ratio of X_1 to X_2 peak heights. These results and those of Ozeki *et al* [19] are convincing evidence for the association of X_1 with Si.

In their earlier work, Wolfe *et al* [17] observed an increase in relative amplitude and broadening of the X_2 peak in their Si doped sample as compared with a control sample grown in the same $AsCl_3$-H_2 reactor. Ozeki *et al* [19] on the basis of a similar increase in amplitude and broadening attributed X_2 to S. Samples doped by adding elemental S to the Ga melt of an $AsCl_3$-H_2 reactor, show a new peak between X_2 and X_3 as shown in Figure 11, but samples doped using H_2S, grown in a similar $AsCl_3$-H_2 system, show only X_1, X_2, and X_3. Asfar *et al* identified S with a peak at lower energy than X_1 in H_2S doped $AsCl_3$-H_2 grown material.

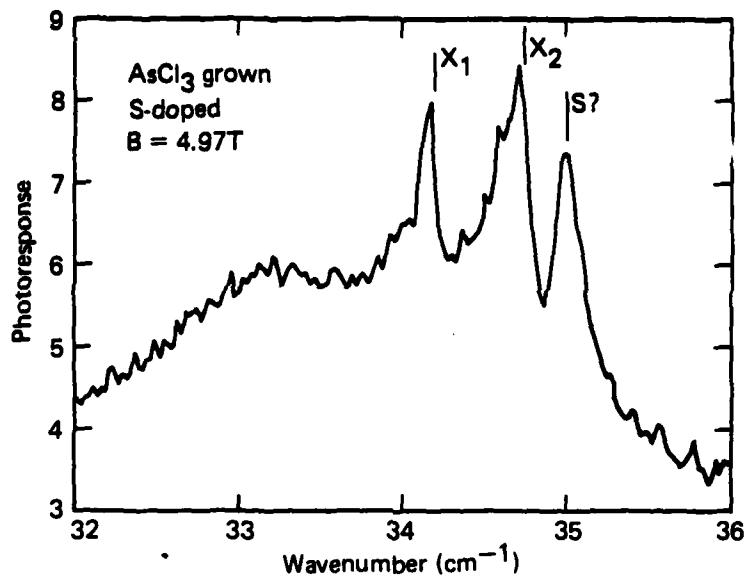

Figure 11. Spectrum for Wolfe's $AsCl_3$-H_2 grown S doped sample.

The peak X_3 was tentatively correlated with C by Wolfe *et al* [17] but Ozeki *et al* [19] concluded that C was not incorporated in GaAs as a donor and observed an increase of the amplitude of this X_3 peak after doping with Ge. Stoelenga *et al* [33] and Asfar *et al* [32] have performed neutron transmutation doping (which is expected to produce only Se and Ge donors) on samples which subsequently showed an increase in the amplitude of the peak X_3. Since the position of the Se peak is well established this is further evidence that X_3 is associated with Ge. The earlier Ge doping experiments of Wolfe *et al* [17] and Cooke *et al* [22] seemed to indicate that the Ge peak occured below X_3 in energy but recent experiments suggest that the peak observed was due to line-shape effects and that the true position of the Ge peak probably coincides with the peak X_3.

Considerable work obviously remains to obtain absolute identification of the donor impurities in GaAs and in particular to identify the source of the residual impurities in the various growth techniques. The present results and identifications pose many interesting and new problems concerning impurity incorporation in epitaxial GaAs. For example, if X_1 is due to Si, then Si is not a significant residual donor impurity in LPE GaAs. If X_3 is due to Ge, neglecting the possible degeneracy of C and Ge, then Ge is the dominant residual donor in MO-CVD GaAs. If X_2 is due to S as identified by Ozeki *et al* [19], then the two other

peaks attributed to S by Stillman *et al* [31] and Asfar *et al* [32] remain unexplained. In spite of these complications and uncertainties, photothermal ionization spectroscopy is the only characterization method that can reliably distinguish and identify the electrically active chemical donor species present in high purity epitaxial GaAs.

5. LINESHAPE ANALYSIS OF PHOTOCONDUCTIVITY SPECTRA

Photoconductivity experiments on high purity GaAs samples are able to detect shallow donor impurities at densities as low as $10^{12}cm^{-3}$ with excellent resolution (especially at high magnetic fields). Thus one might expect this technique to be a powerful spectroscopic tool for the determination of the concentrations of various shallow donor impurities in GaAs as well as for the study of the structure and electrical environment of the shallow donor impurities.

At low temperatures, the principle line broadening mechanism is almost universally believed to be the distribution of electric fields in the sample generated by charged impurities in the crystal. Since the central cell corrections to the shallow donors in GaAs are very small, the separation between lines from different impurities is usually less than the width of the distribution of Stark shifted lines from a specific impurity. However, when a substantial magnetic field is applied, the usually studied 1s-2p transition has no linear Stark shift and the polarizability (or second order Stark shift coupling constant) decreases as the magnetic field increases. Thus, in many cases, lines due to different impurities are easily resolved.

5.1 ANOMALOUS FEATURES

However, many difficulties and discrepancies have arisen in the analysis of photoconductivity data. In the

usual analysis one calculates the distribution of electronic fields in the sample by assuming a random distribution of point charges and then calculates the polarizability of the 1s-2p transition. By combining the two one can easily generate a lineshape that depends only on the density of charged impurities. This parameter can be obtained from Hall and resistivity measurements.

Some of the difficulties and discrepancies found with this procedure are as follows:

(1) The theoretically calculated lineshapes are in very good agreement with the observed lines in many (but not all cases). However, the experimental lines are narrower than the theoretically predicted lines! This is puzzling because while one can always think of additional line broadening mechanisms, it is very difficult to think of line narrowing mechanisms. The usual explanation for this phenomenon is that the positively and negatively charged impurities are not randomly distributed but arrange themselves in such a way as to lessen the random electric fields. While there may be some merit to this idea, it is difficult to see why this mechanism would preserve the lineshape while decreasing the linewidth. This discrepancy could also be produced by an error in the calculation of the polarizability or by an error in the extraction of the density of charged impurities from Hall and resistivity measurements.

(2) Worse yet, in most spectra, lines from different shallow donors have different widths! This is even more puzzling because the Stark shifts should be independent of species. Thus, one is forced to conclude that different types of impurities lie in different regions of charged impurity density. This seems to be an impossible feat of correlation.

(3) In many spectra there are lines whose shapes are different from the usual second order Stark shifted shape. These different lineshapes vary greatly. At one extreme the lines are both broader and more symmetric than second order Stark shifted lines. At the other extreme the lines often look like unresolved or partially resolved doublets. This latter case persists when only one dopant is changed and thus are presumably not due to two different impurity species.

(4) Finally, in measurements with no magnetic field, there is no sharp onset of the 1s-continuum transition. This is somewhat unexpected since the 1s level is broadened only to second order in the electric field and its polarizablity is not very large.

5.2 POSSIBLE MECHANISMS

We are investigating a number of mechanisms in order to remove some or all of these difficulties and inconsistencies. We have not yet addressed the very difficult

problem of the formation of a nonuniform distribution of impurities. Some of the mechanisms that we are considering are complexes, substrate effects, and potential variations.

5.2.1 Complexes

The most exciting part of our work to date is the study of how shallow donor complexes would affect photoconductivity measurements. For the purposes of discussion here, we define a complex as any impurity or defect or combination of impurities and defects that is not a simple substitution of a single Ga or As atom by an impurity with the site symmetry remaining unchanged. Thus any extended defect formed by two or more impurities (including antisite defects and vacancies) is a complex. In addition, any impurity that enters the lattice with a lower symmetry than the atom it replaced is also a complex.

Assuming that a given complex is a shallow donor of charge +e, there must be a vector (or dipole) moment $\vec{d}$ associated with it. Thus $\vec{d}$ would be very small for a substitutional off center defect and quite large for a more extended defect. The energy difference between the 1s and 2p states of the complex, E, will take the form,

$$E = E_o + \alpha_1 \varepsilon^2 + \alpha_2 d^2 + \alpha_3 \varepsilon d ,$$

in the presence of an electric field, ε. All of the quantities above are actually tensors that depend not only on the directions of $\vec{\varepsilon}$ and $\vec{d}$ but also on the

direction of an externally applied magnetic field. We are currently calculating the coefficients, α_i, for a complex with a moment, $\vec{d}$, in the presence of a magnetic field.

Although it is too early to be sure, our theory may explain a number of the anomalies and discrepancies discussed above. For example, for small values of $\vec{d}$, identical complexes could give rise to unresolved or partially resolved lines since α_2 depends on the angle between $\vec{d}$ and the external magnetic field, $\vec{H}$. Further, for large values of d, the term, $\alpha_3 \varepsilon d$, will produce a spectrum that appears to have a first order Stark shift instead of the usual ($\alpha_1 \varepsilon^2$) second order Stark shift.

At least qualitatively, this appears to be consistent with much of the observed data.

5.2.2 Substrate Effects

To our knowledge the effect of substrates on measurements of epitaxial layers has not been considered. Typically, edge effects should be unimportant for sample thicknesses, d, which are much larger than b_i, the average spacing between charged impurities. Here, $b_i \approx n_i^{-1/3}$, where n_i is the density of charged impurities in the sample. In fact, $d >> b_i$ in essentially all samples.

However, n_s, the density of charged impurities in the substrate, can be many orders of magnitude larger than n_i. Our calculations show that substrate effects will be

important in determining photoconductivity lineshapes when

$$d \lesssim n_s/n_i^{4/3}.$$

Typical values for these parameters indicate that this can easily be the case.

It will be significant if the predicted effects do not exist since that would imply useful information about the electrical structure of the substrate.

We are also pursuing calculations as to the effects of charged surface layers.

5.2.3 Potential Variations

We are also investigating the generation and effects of slowly varying potential (as opposed to electric field) variations in a crystal due to a random distribution of charged impurities. Our analysis shows that the characteristic length in the problem is ℓ,

$$\ell = (n_i d)^{-1/2}$$

for a sample of thickness, d, and a density of charged impurities, n_i.

If the Bohr radius, α_o, is much less than ℓ, then all bound states of a donor are shifted by the same amount. However, the energy difference between the 1s state and the continuum will be shifted or smeared by terms of order, α_o/ℓ. This may explain the smearing of the conduction band edge in the photoconductivity experiments.

There are other theories of conduction band and thermal ionization smearing that depend on banding of impurity states. These theories predict dependences that go as $n_i^{-1/3}$. We are currently comparing the various mechanisms.

6. REFERENCES

1. K.H. Nichols, R.E. Goldwasser, and C.M. Wolfe, Appl. Phys. Lett. 36, 602 (1980).

2. P.N. Favennac and H.L'Haridon, Appl. Phys. Lett. 35, 699 (1979).

3. P.M. Asbeck, J. Tandon, B.M. Welch, C.A. Evans, Jr., and V.R. Deline, IEEE Electron Device Lett. 1, 35 (1980).

4. A. Masuyama, M.A. Nicolet, I. Golecki, J.L. Tandon, D.K. Sadana, and J. Washburn, Appl. Phys. Lett. 36, 749 (1980).

5. P.K. Vasudev, R.G. Wilson, and C.A. Evans, Jr., Appl. Phys. Lett. 37, 308 (1980).

6. T.J. Magee, K.S. Lee, R. Ormond, R.J. Blattner, and C.A. Evans, Jr., Appl. Phys. Lett. 37, 447 (1980).

7. T.J. Magee, K.S. Lee, R. Ormond, C.A. Evans, Jr., R.J. Blattner, and C. Hopkins, Appl. Phys. Lett. 37, 635 (1980).

8. F. Simondet, C. Venger, G.M. Martin, and J. Chaumont, Semi-Insulating III-V Materials, (Shiva, Orpington, 1980) p. 100.

9. C.A. Evans, C.G. Hopkins, J.C. Norberg, V.R. Deline, R.J. Blattner, R.G. Wilson, D.M. Jamba, and Y.S. Park, Semi-Insulating III-V Materials, (Shiva, Orpington, 1980) p. 138.

10. P.N. Favennac, M. Gauneau, H. L'Haridon, B. Deveaud, C.A. Evans, Jr., and R.J. Blattner, Appl. Phys. Lett. 38, 271 (1981).

11. T.J. Magee, R.D. Ormond, C.A. Evans, Jr., R.J. Blattner, R.M. Malbon, D.S. Day, and R. Sankaran, Appl. Phys. Lett. 38, 559 (1981).

12. M. Feng, S.P. Kwok, V. Eu, and B.W. Henderson, J. Appl. Phys. 52, 2990 (1981).

13. S.G. Liu, E.C. Douglas, C.P. Wu, C.W. Magee, S.Y. Narayan, S.T. Jolly, F. Kolondra, and S. Jain, (to be published).

14. K.H. Nichols, Camellia M.L. Yee, and C.M. Wolfe, Solid-State Elect. 23, 109 (1980).

15. C.A. Evans, Jr., V.R. Deline, T.W. Sigmon, and A. Lidow, Appl. Phys. Lett. 35, 291 (1979).

16. C.M. Wolfe and G.E. Stillman, Inst. Phys. Conf. Ser. 9, 3 (1970).

17. C.M. Wolfe, G.E. Stillman, and D.M. Korn, Inst. Phys. Conf. Ser. 33b, 120 (1976).

18. K. Dazai, N. Ihara, and M. Ozeki, Fujitsu Sci. Tech. J. 10, 125 (1974).

19. M. Ozeki, K. Kitahara, K. Nakai A. Shibatomi, K. Dazai, S. Okawa, and O. Ryuzan, Japan. J. Appl. Phys. 16, 1617 (1977).

20. J. Kennedy, (private communication).

21. J. Abrokwah, (private communication).

22. R.A. Cooke, R.A. Houlte, R.F. Kirkman, and R.A. Stradling, J. Phys. D. 11, 945 (1978).

23. R.A. Stradling (private communication).

24. S. Tiwari and L.F. Eastman (private communication).

25. H. Morkoç, L.F. Eastman, and D. Woodard, Thin Solid Films 71, 245 (1980).

26. H. Morkoç and A.Y. Cho, J. Appl. Phys. 50, 6413 (1979).

27. D.M. Collins (private communication).

28. A.R. Calawa, Appl. Phys. Lett. 38, 701 (1981).

29. H. Seki, A. Kookitu, K. Ohta, and M. Fujimoto, Japan, J. Appl. Phys. 15, 11 (1976).

30. P.D. Dapkus, K.L. Manasevit, K.L. Hess, T.S. Low, and G.E. Stillman, J. Cryst. Growth (to be published).

31. G.E. Stillman, C.M. Wolfe, and D.M. Korn, Proc 13th Int. Conf. Phys. Semicond. 623, (1976).

32. M.N. Asfar, K.J. Button, and G.L. McCoy, Inst. Phys. Conf. Ser. 56, 547 (1980).

33. J.H.M. Stoelenga, D.M. Larsen, W. Walukiewicz, and C.O. Bozler, J. Phys. Chem. Solids 39, 873 (1978).

7. PUBLICATIONS

1. H. Rohdin, M.W. Muller, and C.M. Wolfe, "Impurity Redistribution During Epitaxial Growth", J. Electron. Mat. (to be published).

8. MEETING TALKS

1. C.M. Wolfe, "Amphoteric Dopants and Compensation in GaAs", Workshop on Shallow Impurities in Semiconductors, Wright-Patterson AFB, Ohio, 21-22 May 1981.

2. G.E. Stillman, "Identification of Shallow Donors in GaAs", Workshop on Shallow Impurities in Semiconductors, Wright-Patterson AFB, Ohio, 21-22 May 1981.

3. H. Rohdin, M.W. Muller, and C.M. Wolfe, "Impurity Redistribution During Epitaxial Growth", Electronic Materials Conference, Santa Barbara, Calif., 24-26 Jun 1981.

9. Distribution List - Annual Technical Report 10/81
Contract N00014-80-C-0762

Code 414 4
Office of Naval Research
Arlington, VA 22217

Naval Research Laboratory
4555 Overlook Avenue, S.W.
Washington, DC 20375
Code 6820 1
6870 1

Defense Documentation Center 12
Building 5, Cameron Station
Alexandria, VA 22314

Dr. Y. S. Park 1
AFWAL/DHR
Building 450
Wright-Patterson AFB
Ohio 45433

ERADCOM 1
DELET-M
Fort Monmouth, NJ 07703

Texas Instruments 1
Central Research Lab
M.S. 134
13500 North Central Expressway
Dallas, TX 75265
Attn: Dr. D. Shaw

Dr. R. M. Malbon/M.S. 1C 1
Avantek, Inc.
3175 Bowers Avenue
Santa Clara, CA 94304

Mr. R. Bierig 1
Raytheon Company
28 Seyon Street
Waltham, MA 02154

Dr. R. Bell, K-101 1
Varian Associates, Inc.
611 Hansen Way
Palo Alto, CA 94304

Dr. Noel Thomas 1
Westinghouse Research And
Development Center
Beulah Road
Pittsburgh, PA 15235

Dr. D. Richard Decker 1
Rockwell International Science Center
P.O. Box 1085
Thousand Oaks, CA 91360

Dr. C. Krumn 1
Hughes Research Laboratory
3011 Malibu Canyon Road
Malibu, CA 90265

Mr. Lothar Wandinger 1
ECOM/AMSEL/TL/IJ
Fort Monmouth, NJ 07703

Dr. Harry Wieder 1
Naval Ocean Systems Center
Code 922
271 Catalina Blvd.
San Diego, CA 92152

Dr. William Lindley 1
MIT
Lincoln Laboratory
F124 A, P.O. Box 73
Lexington, MA 02173

Commander 1
U.S. Army Electronics Command
V. Gelnovatch
(DRSEL-TL-IC)
Fort Monmouth, NJ 07703

RCA 1
Microwave Technology Center
Dr. F. Sterzer
Princeton, NJ 08540

Hewlett-Packard Corporation 1
Dr. Robert Archer
1501 Page Road
Palo Alto, CA 94306

Watkins-Johnson Company 1
E. J. Crescenzi, Jr./K. Niclas
3333 Hillview Avenue
Stanford Industrial Park
Palo Alto, CA 94304

Commandant 1
Marine Corps
Scientific Advisor (Code AX)
Washington, DC 20380

Communications Transistor Corp. 1
Dr. W. Weisenberger
301 Industrial Way
San Carlos, CA 94070

Microwave Associates 1
Northwest Industrial Park
Drs. F. A. Brand/J. Saloom
Burlington, MA 01803

Commander, AFAL 1
AFWAL/AADM
Dr. Don Rees
Wright-Patterson AFB
Ohio 45433

Commander 1
Harry Diamond Laboratories
Mr. Horst W. A. Gerlach
2800 Powder Mill Road
Adelphia, MD 20783

Advisory Group on Electron 1
Devices
201 Varick Street, 11th Floor
New York, NY 10014

Professor L. Eastman 1
Phillips Hall
Cornell University
Ithaca, NY 14853

Professor Hauser and Littlejohn 1
Department of Electrical Engr.
North Carolina State University
Raleigh, NC 27607

Professors Rosenbaum & Wolfe 1
Semiconductor Research Laboratory
Washington University
St. Louis, MO 63130

W. H. Perkins 1
Electronics Lab 3-115/B4
General Electric Company
P.O. Box 4840
Syracuse, NY 13221

Bryan Hill 1
AFWAL/AADE
Wright-Patterson AFB
Ohio 45433

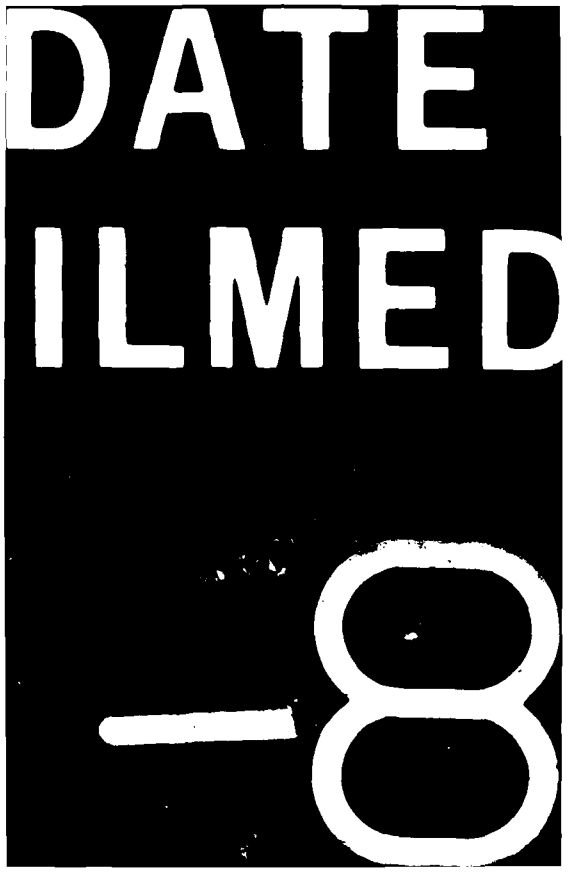
DATE
ILMED
-8